

## On the ridging of intact lead ice

Mark A. Hopkins

Cold Regions Research and Engineering Laboratory, Hanover, New Hampshire

**Abstract.** The sea ice pressure ridging process is modeled using a two-dimensional particle simulation technique. In this model, blocks are broken from an intact sheet of relatively thin lead ice driven against a thick, multiyear floe at a constant speed. The blocks of ice rubble accumulate to form the ridge sail and keel. The energy consumed in ridge growth, including dissipation, is explicitly calculated. A series of numerical experiments are performed to establish the dependence of the energetics on the thickness of the ice sheet and the friction between blocks. The results suggest that the total energy required to create a pressure ridge is an order of magnitude greater than the potential energy in the ridge structure. A typical sea ice cover in the polar regions contains a variety of ice thicknesses that evolve in response to both dynamic and thermodynamic forcing. The variable thickness of the ice cover is created by deformation, which simultaneously causes formation of thick ice through ridge building and thin ice through lead creation. Since the energy expended in deformation is largely determined by the ridging process, an understanding of the energetics of pressure ridging is critical in the determination of ice strength on a geophysical scale.

### Introduction

A framework for describing the variable thickness character of sea ice was developed by *Thorndike et al.* [1975]. Within this framework, pressure ridging is treated statistically by a redistribution process whereby thin ice is transferred to thick ice categories. The increase in potential energy in an area of the ice pack due to pressure ridging can be related to the large-scale strength of the pack ice [*Thorndike et al.*, 1975; *Rothrock*, 1975]. The key issue left unanswered was the magnitude of dissipative losses associated with the potential energy increase. Most estimates have typically placed the total energy losses at about twice the potential energy [see *Rothrock*, 1975], a factor largely based on a kinematic ridge model developed by *Parmeter and Coon* [1972].

Subsequently, in a seasonal simulation of the Arctic basin using a variable thickness sea ice model, *Hibler* [1980] found that unrealistically large ice drift and buildup results were obtained when total energy losses were scaled by a factor of 2 times the potential energy. In a 21-year sensitivity study, *Flato* [1991] found that total energy losses scaled by a factor of 15 times potential energy produced an ice velocity field that compared most closely with observed buoy drifts. Because of the importance of the dissipative energy losses in the ridging process, it is clearly of interest to determine the relative magnitudes of the energetic mechanisms that are a part of ridge formation.

The formation of pressure ridges from existing rubble has been considered by *Sayed and Frederking* [1984] and *Hopkins et al.* [1991]. *Sayed and Frederking* [1984] modeled pressure ridges as triangular wedges of rubble. Assuming that the rubble satisfies the Mohr-Coulomb assumption of a state of uniform failure [*Perloff and Baron*, 1976], *Sayed and Frederking* [1984] derive solutions for the stress distribution

This article is not subject to U.S. copyright. Published in 1994 by the American Geophysical Union.

Paper number 94JC00996.

in the rubble. *Hopkins et al.* [1991] developed a dynamic model, based on a particle simulation, of the compression of a floating layer of ice rubble confined between thick floes. Both works beg the question of the origin of the rubble. The results of the present study will show that a ridge composed of rubble need not be built from rubble.

In the present work, pressure ridges are grown from a sheet of intact, relatively thin, first-year ice. The sheet is pushed with constant speed against a thick, multiyear floe. The sheet breaks repeatedly in flexure, creating the blocks which form the ridge sail and keel. This type of ridge growth violates the Mohr-Coulomb assumption of uniform failure because of the discrete and local nature of the failure zone surrounding the intact sheet and because the ridge structure, once formed, is largely static. Preliminary results using a less sophisticated model of this type were presented by *Hopkins and Hibler* [1991]. The main assumption in the present study is that the ice sheet breaks in flexure (including buckling). Therefore the results do not apply to ice thicknesses wherein the primary failure mechanism is crushing.

### Dynamic Ridge Model

The dynamic ridge model is based on the particle simulation technique. A particle simulation is a computer program which explicitly models the dynamics of a system of discrete particles, henceforth called blocks. The position, orientation, velocity, and shape of each block are stored in arrays. At each time step the contact and body forces on each block are calculated, and the blocks are moved to new locations with new velocities that depend on the resultant of the forces.

The important features of the ridge model are a dynamic, linear viscous elastic model of a floating ice sheet; flexural failure (including buckling) of the ice sheets; realistic block lengths broken from the parent sheet at points where tensile stress exceeds strength; secondary flexural breakage of rubble blocks; inelastic contacts between rubble blocks;

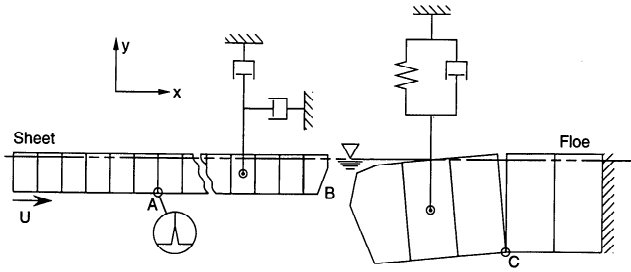


**Figure 1.** Discretization of the floe and lead ice sheet into uniform rectangular blocks, showing the boundary conditions on the lead ice sheet and floe. Skeletal layer is modeled by terminating the viscous elastic joint between adjacent blocks (point A). The tip of the sheet is bevelled (point B) to facilitate the sheet riding up the floe or over rubble blocks. The pin joint (point C) constrains the motion of a broken floe.

frictional sliding contacts between blocks; separate friction coefficients for submerged and above-water contacts; buoyancy of the ice sheets and rubble; and water drag. The key assumption in this study is that the ice sheet breaks in flexure. Therefore the conclusions should not be applied to ice thicknesses wherein the primary failure mechanism is crushing. The description of the important features of the ridge model follows. A detailed description is provided by Hopkins [1992].

This work is based on a concept of ridge growth in which an intact sheet of thin ice is driven against a thick ice floe. The approach used to model the dynamic behavior of the intact ice sheet is akin to an explicit, finite difference technique. The thin ice sheet and rubble blocks, broken from the sheet, are each composed of single rows of uniform, rectangular blocks that are attached to neighboring blocks by viscous elastic joints. The discretization of the floating ice sheet is shown in Figure 1. Relative displacements between adjacent blocks create forces and moments, internal to the sheet and rubble blocks, which act on the individual, component blocks. The internal forces on the component blocks are added to external forces exerted by the surrounding ice rubble, gravity, and buoyancy. When the tensile stress in a joint at either surface of the sheet or a rubble block exceeds the specified strength, a crack is initiated. The crack propagates at constant speed across the joint, requiring many time steps for completion. The block created by the fracture becomes part of the rubble and is added to the ridge structure. While the cracks must occur at joints, the length of the rubble blocks is variable since they may contain any number of component blocks.

Temperature and salinity gradients are present in an ice sheet because the top surface is exposed to air and the bottom surface is submerged. These gradients produce a variation in the stiffness and tensile strength through the sheet. This variation is qualitatively modeled by using an elastic modulus, which varies linearly through the sheet, and separate values of the tensile strength at the top and bottom surfaces. In addition, there is a weak layer of extremely saline ice, several centimeters thick, at the bottom surface of an ice sheet. The skeletal layer is modeled by terminating the viscous elastic joint between the rectangular blocks several centimeters above the bottom surface as shown in Figure 1 at point A.

The uniform, rectangular blocks which compose the sheet and rubble are connected by viscous elastic fibers. The width of a block is  $W$ , and the height is  $h$ , the thickness of the parent sheet. (The depth of the blocks and, indeed, of the entire simulation is 1 m.) Relative motion between adjacent blocks, assumed small in relation to the size of the blocks, produces tensile and compressive forces between blocks. A pair of blocks that have rotated with respect to one another is shown in Figure 2. The vector  $\delta(t)$  shown in Figure 2 represents a stretched fiber. It is defined by the position of a point on block  $j$  with respect to the adjacent point on block  $i$  in the undeformed state. A local  $n, t$  coordinate frame is shown with its origin at the center of the face of block  $i$ .

The normal stress at a point  $t$  on the joint has an elastic and a viscous component. The elastic component is  $E(t)\delta_n(t)/W$ . The elastic modulus  $E(t)$  varies linearly in the tangential direction along the joint. The viscous component is  $\eta(t)\dot{\delta}_n(t)$ . The viscosity coefficient  $\eta(t)$  used in the experiments is 10% of the critical damping value  $2(\rho_i E(t))^{1/2}$ . The total normal force  $F_n$  is found by integrating the two components over the length of the joint

$$F_n = \int E(t)\delta_n(t)/W + \eta(t)\dot{\delta}_n(t) dt \quad (1)$$

Similar expressions are derived for the tangential (shear) forces and moments. The shear modulus is derived from the elastic modulus and Poisson's ratio as  $G = E/2(1 + \nu)$ . The shear stiffness  $k_{te}$  is  $G/W$ . The thick floe is also discretized and treated similarly.

Equation (1) and similar expressions for the tangential forces and moments are used to model the internal forces due to compression and flexure of the sheet, floe, and individual rubble blocks. External, contact forces such as those between rubble blocks, between rubble and sheet or floe, or between sheet and floe use a different force model which supports no tensile force. Two blocks are defined to be in contact if the polygons defining their shapes intersect. The force between two intersecting blocks is defined in a local  $n, t$  coordinate frame defined by the normal to a contact surface connecting the intersection points. The force acts at the centroid of the area of intersection. A viscous elastic normal force model is used with a Coulomb friction, tangential force model. A simple representation of the normal component of the contact force model is shown in Figure 3. The elastic component of the normal force  $F_{ne}$  is

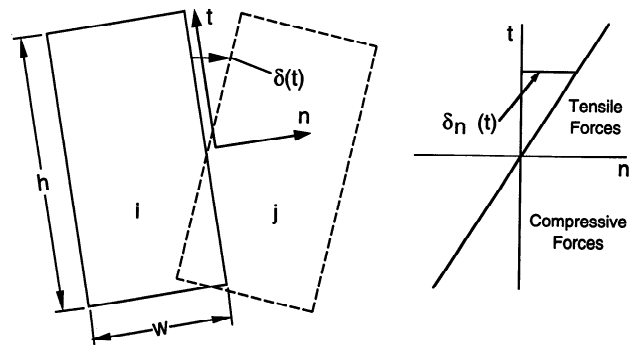


**Figure 2.** (left) Pair of adjacent blocks from a point at which the ice sheet is in flexure, (right) showing the local coordinate frame with regions in tension and compression.

$$F_{ne}^n = k_{ne} \text{Area}^n \quad (2)$$

where the superscript  $n$  denotes the current time step,  $\text{Area}^n$  is the current area of intersection, and  $k_{ne}$  is the normal elastic stiffness. The viscous component of the normal force  $F_{nv}$  is

$$F_{nv}^n = k_{nv}(\text{Area}^n - \text{Area}^{n-1})/\Delta t \quad (3)$$

where  $\Delta t$  is the time step. The viscous damping constant  $k_{nv}$ , used to create highly inelastic behavior at contacts between rubble blocks, is 50% of the critical damping value  $2(k_{ne}h\rho_i)^{1/2}$ , where  $h$  is the thickness and  $\rho_i$  the density of the parent sheet.

A representation of the tangential contact force model is shown in Figure 4. The tangential force  $F_t$  increases due to incremental slip between the polygons at the contact surface in the tangential direction [Walton, 1980]. The incremental slip occurring between the polygons from time step to time step creates the tangential force by compressing the spring in Figure 4. The tangential force is

$$F_t^n = F_t^{n-1} - k_{te}\Delta t (V_{ij}^{n-1/2}) \quad (4)$$

where  $k_{te}$  is the tangential elastic stiffness and  $V_{ij}$  is the relative velocity between the pair of polygons at the centroid of the overlapping area. The magnitude of the tangential force is not allowed to exceed  $\mu F_n$ , where  $\mu$  is the coefficient of friction. When the tangential force reaches the Coulomb limit, sliding occurs.

The internal forces and moments at each joint in the ice sheet, floe, and rubble blocks and the external, contact forces between blocks are calculated at each time step. The resultant of the internal and external forces on each block is calculated. Equations of motion, derived from a Taylor series expansion about the current time, are used to find the updated positions and velocities. The  $x$  component of velocity  $u^{n+1/2}$  of polygon  $i$  is

$$u_i^{n+1/2} = u_i^{n-1/2} + \Delta t F_{xi}^n/\text{mass}_i \quad (5)$$

where  $F_{xi}$  is the  $x$  component of the resultant force on block  $i$ . The  $x$  coordinate of polygon  $i$  at time  $n + 1$  is then

$$x_i^{n+1} = x_i^n + \Delta t u_i^{n+1/2} \quad (6)$$

Similar equations are used for the  $y$  component of velocity  $v$ , the  $y$  coordinate, the angular velocity  $\omega$ , and the orientation  $\theta$ .

**Boundary Conditions on the Sheet and Floe**

The boundary conditions imposed on the thin ice sheet are illustrated in Figure 1. The first (leftmost) block of the sheet

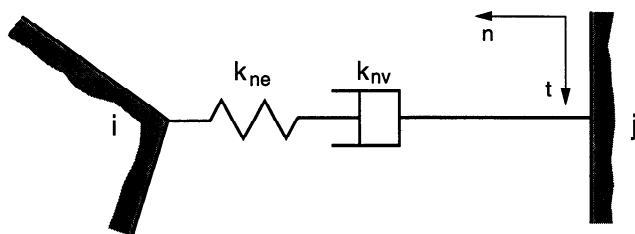


Figure 3. Normal direction contact force model.

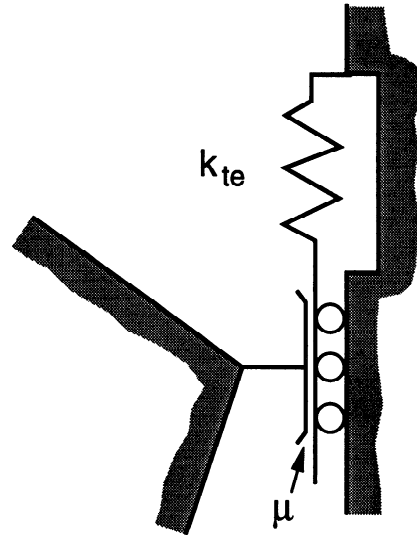


Figure 4. Tangential direction contact force model.

moves with constant speed  $U$  in the positive  $x$  direction for the duration of an experiment. Because of deformation, the rest of the sheet does not generally move at the same speed. The sheet length is kept constant by adding blocks to the left end as blocks are broken from the right end.

The weak, skeletal layer at the bottom of the sheet, discussed above, is implemented by terminating the elastic joint between adjacent blocks above the bottom of the sheet. This is shown, magnified, in Figure 1, inset at point A. The typical thickness of this layer in the experiments was 4 to 6 cm. The tip of the sheet at Figure 1, point B, is beveled to facilitate the sheet riding up the floe or over rubble blocks. The four corners of blocks broken from the sheet are beveled 2 cm at a 45° angle.

A viscous force is imposed on each block composing the thin sheet in order to qualitatively simulate the support and damping characteristics of a three-dimensional sheet and the damping effects of the water. The  $x$  and  $y$  components (in the global coordinate frame) of the force are

$$F_{xv} = -k'_{nv}(u_i - u_1) \quad (7)$$

$$F_{yv} = -k'_{nv}v_i$$

where  $u_i$  and  $v_i$  are the  $x$  and  $y$  velocity components of block  $i$ . The effective viscosity coefficient  $k'_{nv}$  on block  $i$  is

$$k'_{nv} = k_{nv}e^{-4(x_i - x_1)/(x_n - x_1)} \quad (8)$$

where  $x_n$  is the  $x$  coordinate of the rightmost and  $x_1$  is the  $x$  coordinate of the leftmost block in the sheet. The exponential decay of the viscous constant is designed to dissipate energy which would otherwise cause destructive oscillations at the left end of the sheet. The constant 4, which determines the rate of exponential decay, was arrived at empirically. Constants less than 3 produced extremely brittle behavior in the ice sheet, whereas constants greater than 5 allowed the sheet to move too freely. Although these viscous boundary conditions are qualitative, the buoyancy of the sheet and ice rubble are rigorously modeled by calculating their submerged area.

In order to qualitatively simulate the lateral support that a

three-dimensional floe would provide and the oscillation damping effects of the water, a viscous elastic force, illustrated by a spring and dashpot in Figure 1, is imposed on each block composing the floe. The value of the elastic stiffness was chosen to limit the subsidence of a broken floe to a reasonable value of a half meter or less. The motion of a broken floe is constrained by a pin joint shown in Figure 1 at point C. The beveling of the nose of the floe, to enable ride up, is also shown.

### Energetics

The work performed by the moving ice sheet is transformed into the potential energy of the ridge structure or dissipated. Dissipative mechanisms consist of frictional and inelastic contacts and water drag. The work, calculated from the force required to push the sheet, is compared to the sum of the potential energy, kinetic energy, and dissipation terms to gauge the numerical accuracy of the simulation. In the experiments discussed below the difference between the calculated work and the sum of the energy sinks was less than 1%. All of the components of the energy budget are measured in watts per meter of ridge width.

The force required to push the ice sheet at a constant speed is equal to the sum of the horizontal forces exerted on the sheet by the rubble. Therefore the work required to build the ridge is

$$\text{work} = u_{\text{sheet}} \Delta t \sum_n \sum_i F_{xi}^n \quad (9)$$

The summations in (9) are over the  $x$  components of the forces exerted by the rubble on the thin sheet  $\sum_i$  at each time step  $\sum_n$  in the experiment. The change in the potential energy of the ridge structure is

$$\Delta PE = g \Delta t \sum_n \sum_i (v_i^n \rho_i A_i - v_{is}^n \rho_w A_{is}^n) \quad (10)$$

The summations in (10) are over each block in the sheet, floe, and rubble at each time step.  $A_i$  is the area, and  $v_i$  is the vertical component of the velocity of block  $i$ .  $A_{is}$  is the submerged area, and  $v_{is}$  is the vertical component of the velocity of the center of mass of the submerged area of block  $i$ . The acceleration of gravity is  $g$ , the ice density is  $\rho_i$ , and the water density is  $\rho_w$ . The frictional dissipation  $\Phi_f$ , which is the work performed by the tangential contact forces at each point of contact, is

$$\Phi_f = \Delta t \sum_n \sum_i (F_t^n V_{1/2}^n)_i \quad (11)$$

Similarly, the dissipation  $\Phi_i$  caused by viscous damping, which controls inelasticity, is the net work performed by the normal contact forces at each point of contact

$$\Phi_i = \Delta t \sum_n \sum_i (F_n^n V_{1/2}^n)_i \quad (12)$$

The summations in (11) and (12) are over all pairs of blocks in contact  $i$  at each time step  $n$ .  $V_{1/2}$  is the relative velocity at the contact point. The normal and tangential force components are given by (2)–(4). Other energy sinks are kinetic energy and energy dissipated by water drag and viscous

**Table 1.** Parameters Used in the Experiments

Parameter	Value
Floe thickness	2, 3 m
$h$ (ice sheet thickness)	20, 25, 30, 35, 40, 45 cm
Ice sheet speed	6.25, 25 cm s <sup>-1</sup>
$W$ (sheet block width)	20 ( $h = 20$ ), 25, 30 ( $h = 45$ ) cm
Skeletal layer	20% of thickness to maximum of 6 cm
Elastic moduli	
Floe top	1.0 GPa
Floe bottom	0.67 GPa
Lead top	0.1, 0.4, 1.0 GPa
Lead bottom	0.067, 0.267, 0.67 GPa
$\nu$ (Poisson's ratio)	0.3
Tensile strength sheet (top)	750 kPa
Tensile strength sheet (bottom)	350 kPa
$\rho_i$ (ice density)	920 kg m <sup>-3</sup>
$\rho_w$ (water density)	1010 kg m <sup>-3</sup>
$\mu$ (dry friction)	0.4, 0.6, 0.8, 1.0
$\mu_w$ (wet friction)	0.3, 0.6
$k_{ne}$ (normal contact stiffness)	10 <sup>8</sup> N m <sup>3</sup>

boundary forces which, in total, typically amount to less than 5% of the energy consumed.

### Numerical Ridge Growth Experiments

A series of experiments were performed to determine the effects of various parameters on the ridge structure and the energetics of the ridging process. The parameters examined were the friction between ice blocks, ice thickness, the elastic modulus, and the speed of the sheet. Separate friction coefficients  $\mu$  and  $\mu_w$  were used for above-water and submerged contacts, respectively. In each experiment, 100 m of ice was pushed into the ridge. The parameters used in the experiments are listed in Table 1. The tangential stiffness coefficient in rubble contacts  $k_{te}$  was 60% of the normal value. The normal viscosity coefficient  $k_{nv}$  was 50% of the critical damping value  $2(k_{ne} h \rho_i)^{1/2}$ .

The ridge growth experiments begin with an intact sheet of thin ice driven against a thick, multiyear ice floe at a constant speed. The discretization of the ice sheet and floe into rectangular component blocks is shown in Figure 1. As the ice sheet collides with the floe, it fails, creating rubble blocks that accumulate to form the ridge structure. The pile of blocks on the floe form the ridge sail. The submerged pile forms the keel. A sequence of snapshots from a numerical experiment performed with the simulation using 30-cm lead ice and 2-m thick floe ice is shown in Figure 5. The friction coefficients were  $\mu = 1.0$  and  $\mu_w = 0.6$ . The times in the snapshots are in seconds, with the sheet moving at 25 cm s<sup>-1</sup>. Each snapshot encloses an area 20 m wide by 12 m high.

Sail growth takes place by direct piling of blocks pushed by the sheet onto the floe. The blocks, broken in succession from the sheet, form a train climbing the leadward side of the sail. The force required to push the blocks depends on the height and slope of the sail and the friction between sliding blocks. The part of the ridge keel, in front of the floe, functions as a platform supporting the downward component of the sail-building force. Sail growth continues as long as the sheet is able to transmit the force and the platform is able

to support the downward component. If the sheet is unable to transmit the force, it buckles. If the platform is unable to support the force, it collapses. In general, ridge growth exhibits a cyclic alternation between sail growth and platform growth.

Rubble is added to the keel at the surface when the progress of the sheet, sliding across the platform, is momentarily obstructed, causing it to buckle or break in flexure. Blocks are also added to the keel when the leadward part of the sail becomes unstable and collapses into the platform. As the keel grows, it spreads in both directions like an inverted pile. The spreading pile is continually pushed in the direction of the floe by the motion of the sheet. Occasionally, the

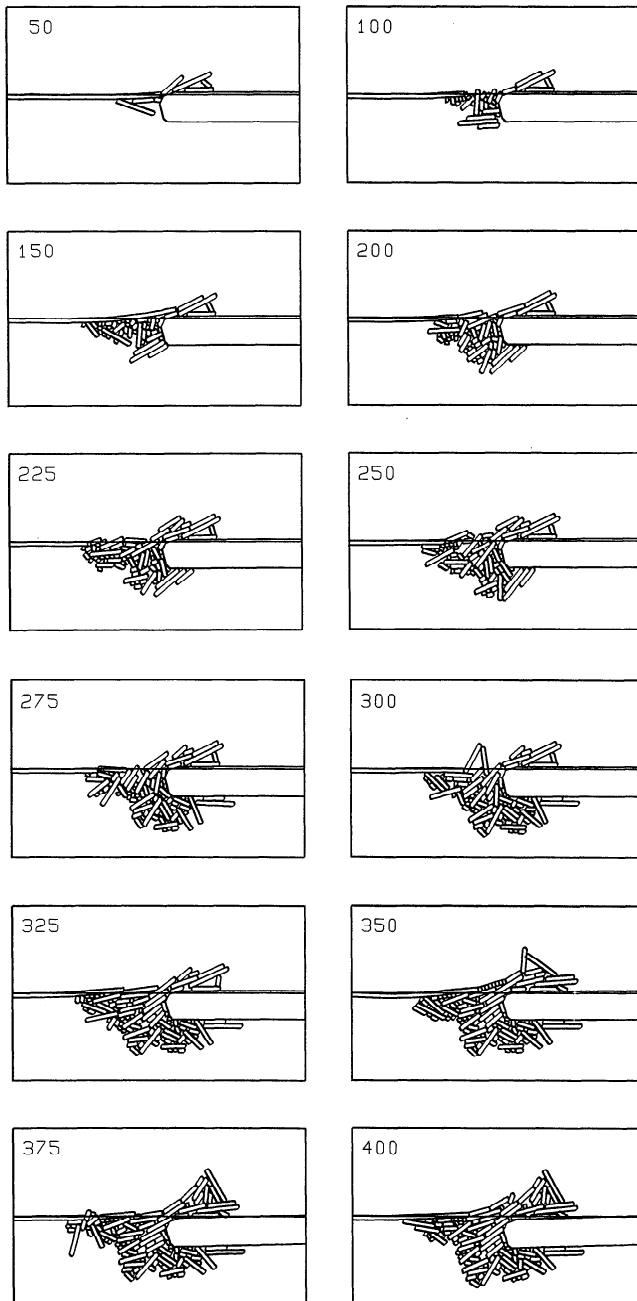


**Figure 5.** Sequential snapshots from a ridging experiment. The ice thickness was 30 cm, and the friction coefficients were  $\mu = 1.0$  and  $\mu_w = 0.6$ . Each frame is 12 m  $\times$  20 m.

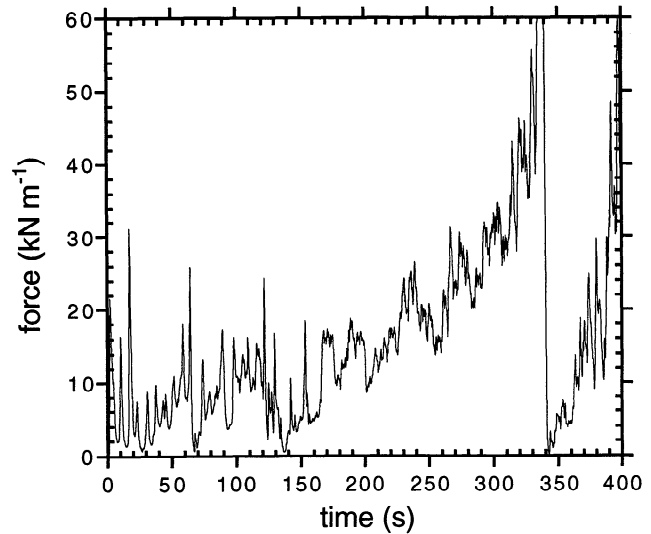


**Figure 6a.** Force (kilonewtons per meter) versus time from an experiment with low-friction ice. The ice thickness was 30 cm, and the friction coefficients were  $\mu = 0.4$  and  $\mu_w = 0.6$ .

sheet, deflected downward, shoves submerged rubble beneath the floe.

During the experiments the ridge-building force, the total energy consumed (see (9)), the potential energy of the ridge structure (see (10)), and the energy lost to frictional (see (11)) and inelastic dissipation (see (12)) are continually calculated. The variation of the ridge-building force (per meter) with time is shown in Figures 6a and 6b. The force was sampled at 0.2-s intervals. Figure 6a is from an experiment with low-friction ice. The period from 0 to 70 s, characterized by sharp spikes, was a period of keel building. The periods from 70 s to 135 s, 140 s to 340 s, and 350 s to 400 s, characterized by sustained forces, were periods of sail building. Figure 6b is from the experiment shown in Figure 5 with high-friction ice. The periods from 60 s to 190 s and 223 s to 317 s, characterized by sharp spikes in the force plot, were periods

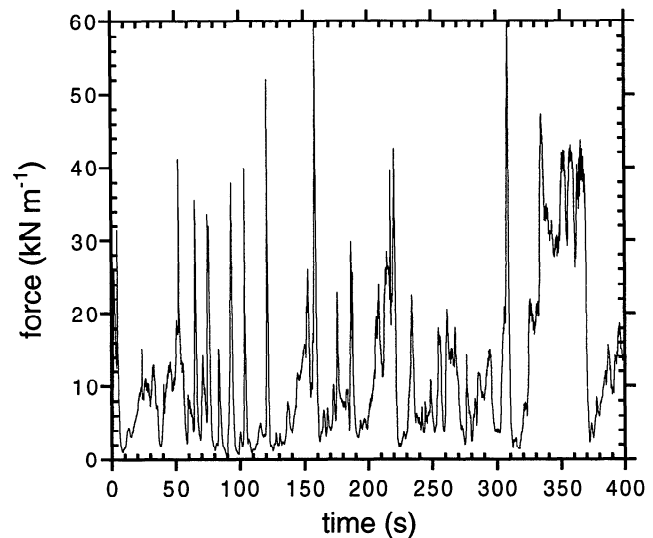


**Figure 6b.** Force (kilonewtons per meter) versus time from the experiment with high-friction ice shown in Figure 5.

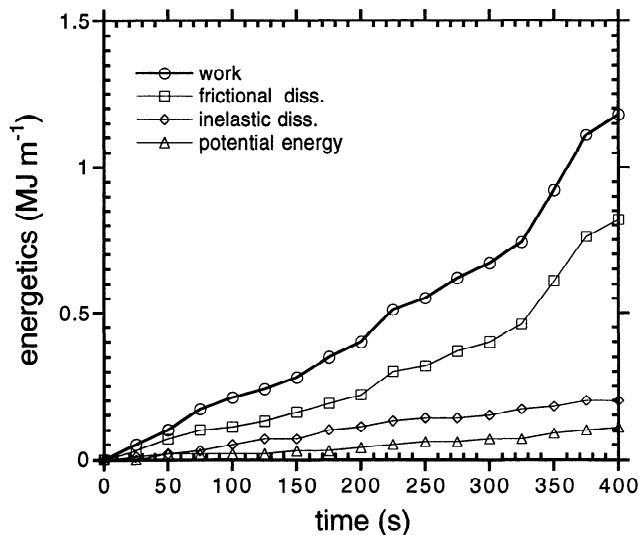


Figure 7. Energy budget (megajoules per meter) of the experiment shown in Figure 5.

of keel building. The periods from 10 s to 50 s, 190 s to 220 s, and 317 s to 372 s, characterized by relatively sustained forces, were periods of sail building. The spikes during periods of keel building accompany buckling.

The energetics of the ridging simulation pictured in Figure 5 are shown in Figure 7. The plot shows the relative magnitudes of the various sinks with respect to the total work required to build the ridge. Frictional dissipation is, by far, the largest energy sink, dissipating about 8 times more energy than remains as potential energy in the final structure.

A random variation ( $\pm 1\%$ ) in the elastic modulus at each joint in the thin ice sheet was used to create unique outcomes in experiments using the same initial configuration of ice and the same set of parameters. This small variation was sufficient to cause the experiments to diverge noticeably by the time several blocks had been broken from the parent sheet. In numerical experiments to determine the effects of various parameters, which are discussed below, the averages of sets of seven experiments with each set of parameters are compared.

Two sets of experiments were run to assess the effects of variations in the lead ice sheet velocity. The two velocities tested were  $6.25 \text{ cm s}^{-1}$  and  $25 \text{ cm s}^{-1}$ . The average final ridge profiles and energetics in the two sets of experiments were nearly identical. The inelastic dissipation increased slightly at  $25 \text{ cm s}^{-1}$ , and frictional dissipation decreased by an equal amount. In the interest of computational speed all subsequent experiments were run at  $25 \text{ cm s}^{-1}$ .

Three sets of experiments were run to assess the effects of variations in the elastic modulus of the lead ice sheet. The values tested for the modulus at the top of the sheet were 0.1, 0.4, and 1.0 GPa. The moduli at the bottom of the sheet were  $2/3$  of the top values to qualitatively account for temperature and salinity variations. These values are somewhat lower than published values [Mellor, 1986] that fall in the 1.0 to 10.0 GPa range, depending on temperature and deformation rate. In experiments performed with the higher values the ice sheet appeared noticeably more brittle than in the test at the lowest value and the blocks were somewhat

smaller. The average energy consumed using the highest modulus was 10% lower than for the lowest modulus, which is probably due to the smaller block size. Breakage, per se, consumed little energy. There were no significant differences between the final profiles. Since the differences were not large and the simulation time step is inversely proportional to the square root of the modulus, the value 0.1 GPa was used for the remaining experiments.

Two sets of experiments were performed with 2-m and 3-m thick floes. As expected, less ice was forced beneath the thicker floe. However, there was no significant effect on the energetics due to floe thickness. All other experiments used a 2-m thick floe.

### Effects of Friction

Frictional contacts dissipate energy when one block slides across another. In experiments performed with the ridging model, frictional dissipation is the largest energy sink. The model uses two friction coefficients,  $\mu$  for above-water contacts and  $\mu_w$  for submerged contacts. The coefficients are considered to be "effective" values which include the effects of macroscopic roughness and incipient freezing. The selection of reasonable values of the friction coefficients for the experiments was hampered by the lack of field data. Laboratory measurements of friction between smooth ice blocks are not relevant because of the absence of macroscopic roughness. In lieu of useful empirical data, eight sets of experiments were performed with various combinations of  $\mu$  and  $\mu_w$ . In the experiments the lead ice thickness was 30 cm, the velocity was  $25 \text{ cm s}^{-1}$ , and the duration was 400 s.

Seven experiments were performed with each combination of  $\mu$  and  $\mu_w$ . Average ridge profiles were constructed by dividing individual profiles into meter-wide vertical strips. The mean height and depth of ice in each strip were calculated and averaged over each set of seven experiments. The average final ridge profile, for each combination of  $\mu$  and  $\mu_w$ , is shown in Figure 8. Each box encloses an area 22 m wide by 11 m high. It is apparent from the profiles that increasing the above-water coefficient of friction  $\mu$  results in a smaller, more compact sail and a larger keel. Experiments with  $\mu$  less than 0.4 resulted in sails of enormous widths. Increasing the underwater coefficient  $\mu_w$  had little effect. The structural effect of  $\mu$  on the relative volume of sail and keel is caused by the limit on the sail-building force due to buckling.

The force required to enlarge a ridge sail increases with the magnitude of the friction coefficient  $\mu$  and the size of the ridge sail. The magnitude of the sail-building force is limited by the ability of the sheet to resist buckling. Because the sheet tip is constrained by surrounding ice rubble, the buckling force is nearly independent of  $\mu$ . Since the available force is limited, increasing  $\mu$  will cause a reduction in sail size. Furthermore, since the supply of rubble remains constant, a reduction in sail volume will be accompanied by an increase in keel volume.

The results in Table 2 describe the average energy budget in each set of experiments with a given combination of  $\mu$  and  $\mu_w$ . The components of the energy budget are explicitly calculated during the experiments using (9)–(12). The small difference between the total energy consumption or work and the sum of the other components given in Table 2

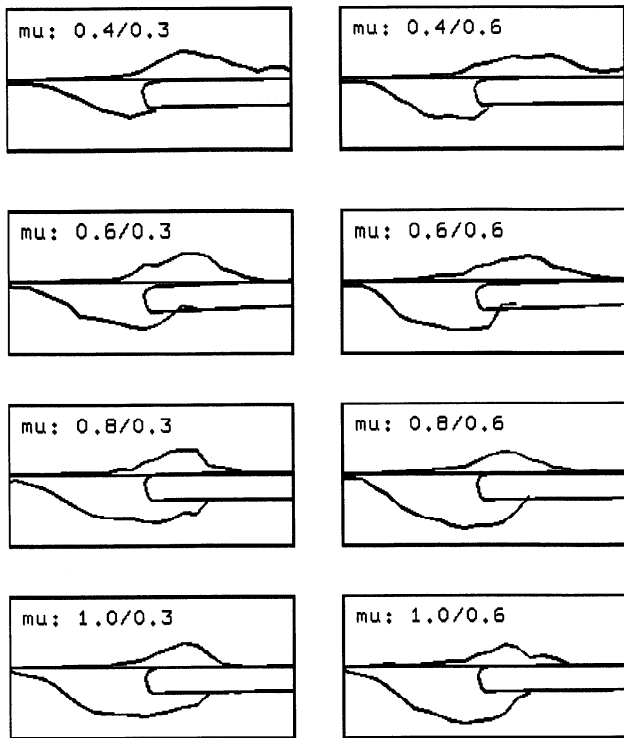


Figure 8. Averaged final ridge profiles from eight sets of experiments using different values of friction coefficients.

represents energy lost to water drag, kinetic energy, and calculation error (all small quantities). The results show a decrease in work, frictional dissipation, and potential energy as  $\mu$  is increased. The average work as a function of the volume of ridged ice, for each combination of  $\mu$  and  $\mu_w$ , is plotted in Figure 9. The results in Figure 9 also show that energy consumption is inversely related to  $\mu$ .

If ridge building proceeded in an orderly manner, with blocks pushed by the sheet sliding smoothly over the layer beneath, then energy consumption would increase with  $\mu$ . The opposite relationship between energy consumption and friction suggests that the ridging process becomes less orderly as  $\mu$  increases. Figures 6a and 6b show the instantaneous ridging force as a function of time from typical experiments with low- and high-friction ice. In Figure 6a the

Table 2. Major Components of the Energy Budget Averaged Over Seven Experiments With Each Set of Friction Coefficients

$\mu$	$\mu_w$	Work	$\Phi_f$	$\Phi_i$	$\Delta PE$	$W/\Delta PE$
1.0	0.6	1.170	0.870	0.171	0.084	13.9
0.8	0.6	1.182	0.861	0.183	0.084	14.1
0.6	0.6	1.329	0.984	0.192	0.102	13.0
0.4	0.6	1.389	1.080	0.189	0.132	10.5
1.0	0.3	1.041	0.765	0.156	0.081	12.9
0.8	0.3	1.017	0.780	0.126	0.087	11.7
0.6	0.3	1.116	0.837	0.135	0.105	10.6
0.4	0.3	1.203	0.966	0.135	0.126	9.6

Major components of the energy budget are computed in megajoules per meter. Abbreviations include  $\mu$ , friction coefficient for above-water contacts;  $\mu_w$ , friction coefficient for submerged contacts;  $\Phi_f$ , frictional dissipation;  $\Phi_i$ , viscous dissipation;  $\Delta PE$ , change in potential energy; and  $W/\Delta PE$ , ratio of work to  $\Delta PE$ .

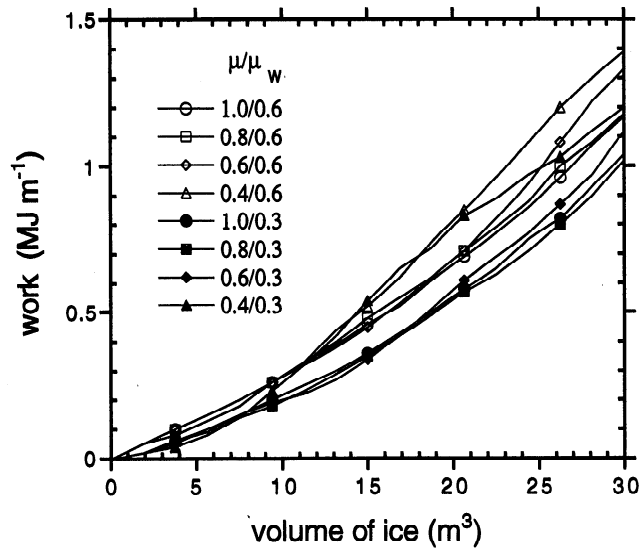


Figure 9. Total energy consumption (megajoules per meter) versus volume of ridged ice from the averaged results of eight sets of experiments with various friction coefficients.

ridging force exhibits long periods of continuous increase, characteristic of sail building. In Figure 6b there are many high peaks in the force, followed by sharp drops caused by buckling. Since the sheet velocity is constant, total energy consumption is proportional to the average force. Thus increasing  $\mu$  has the paradoxical effect of increasing the peak forces while lowering the average force.

On the basis of the results of these experiments, increasing friction decreases sail volume relative to keel volume, lowers the total energy consumption, and increases the ratio of work to potential energy. In the absence of field measurements of friction coefficients it is hard to say which combination of coefficients yields the most realistic results. However, on the basis of field measurements of ridge profiles [Kovacs, 1972], the compact sails and balanced structure formed of high-friction ice may be more realistic than the sprawling sails and small keels formed from low-friction ice. Therefore in the next series of experiments, which explore the effects of thickness variations, values of  $\mu = 1.0$  and  $\mu_w = 0.6$  are used. In any case, the difference in energy consumption between the high- and low-friction experiments for a given value of  $\mu_w$  was only about 15%.

### Effects of Lead Ice Thickness

Six sets of experiments were performed to assess the effects of variations in the thickness of the lead ice sheet. The average profile for each set of experiments is shown in Figure 10. Since the duration and ice sheet speed in each set of experiments are the same, the volume of ice in each ridge is proportional to thickness. The width and depth of the keel increase with volume. The average energy budget for the six sets of experiments is shown in Table 3.

Figure 11 shows the average work as a function of the volume of ridged ice for each of the six sets of experiments. These results suggest that the dependence of energetics on thickness may be, more generally, expressed in terms of the volume of ridged ice. However, this conclusion must be qualified.

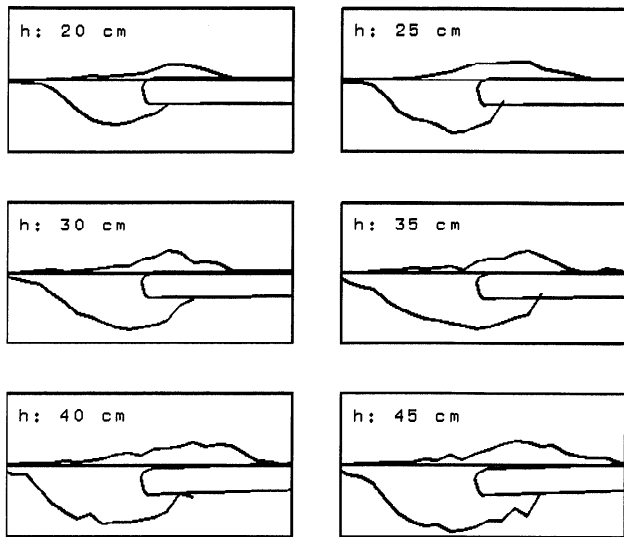


Figure 10. Averaged final ridge profiles from six sets of experiments using different thicknesses of lead ice. The experiments used friction coefficients  $\mu$  and  $\mu_w$  of 1.0 and 0.6, respectively.

The experiments consider only what might be termed primary ridge growth, the period before the ridge sail reaches its maximum height. Sail growth is ultimately limited by the ability of the lead ice to transmit the sail-building force. When this limit is reached, the ridging process enters a second stage, exclusively devoted to keel growth. Since keel building requires less energy than sail building, plots of energy consumption versus ice volume, for ice of a given thickness, would deviate from the general trend shown in Figure 11. The transition point, in terms of the volume of ridged ice, would depend on sheet strength or thickness.

The total ridge-building work as a function of the volume of ridged ice from individual experiments with six thicknesses of lead ice sampled at 25-s intervals is plotted as points in Figure 12. The central line through the data is a quadratic equation

$$\text{Work} = V(463.90V + 26126) \quad (13)$$

obtained by a least squares regression. The upper and lower lines are bounds that define the 95% confidence interval. An equation for the potential energy in the ridge structure

$$PE = V(30.88V + 2107.26) \quad (14)$$

Table 3. Major Components of the Energy Budget Averaged Over Seven Experiments With Each Ice Thickness

$h$	Vol	Work	$\Phi_f$	$\Phi_i$	$\Delta PE$	$W/\Delta PE$
0.20	20	0.705	0.585	0.090	0.042	16.8
0.25	25	1.026	0.801	0.144	0.069	14.9
0.30	30	1.170	0.870	0.171	0.084	13.9
0.35	35	1.347	0.960	0.228	0.090	15.0
0.40	40	1.755	1.218	0.342	0.132	13.3
0.45	45	2.124	1.461	0.456	0.159	13.4

Abbreviations and values are same as for Table 2, and additional ones are  $h$ , ice thickness in meters and vol, ice volume in cubic meters.

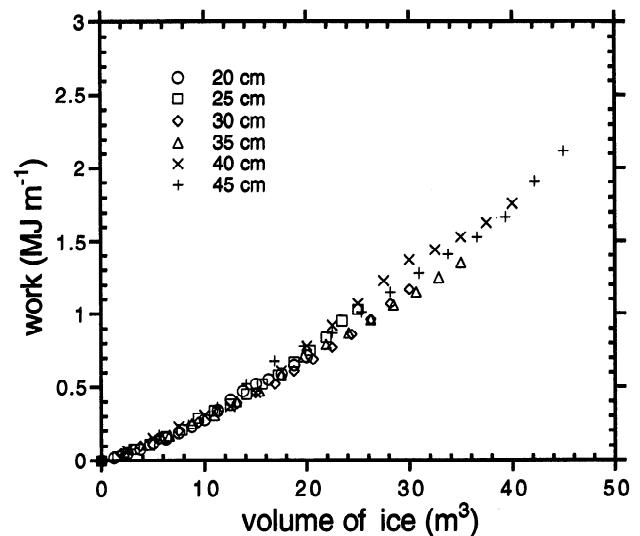


Figure 11. Total energy consumption (megajoules per meter) versus volume of ridged ice from the averaged results of six sets of experiments with lead ice of different thicknesses.

was obtained in a similar manner. The rate of work in ridging is given by the time derivative of (13). Expressing ice volume as the product of ice sheet velocity, thickness  $h$ , and time and expressing the rate of work as the product of force and sheet velocity yields an equation for the average ridging force,

$$\text{Force} = h(927.80V + 26126). \quad (15)$$

The ratio of the rate of work to the rate of increase in potential energy is the ratio of the derivatives of (13) and (14),

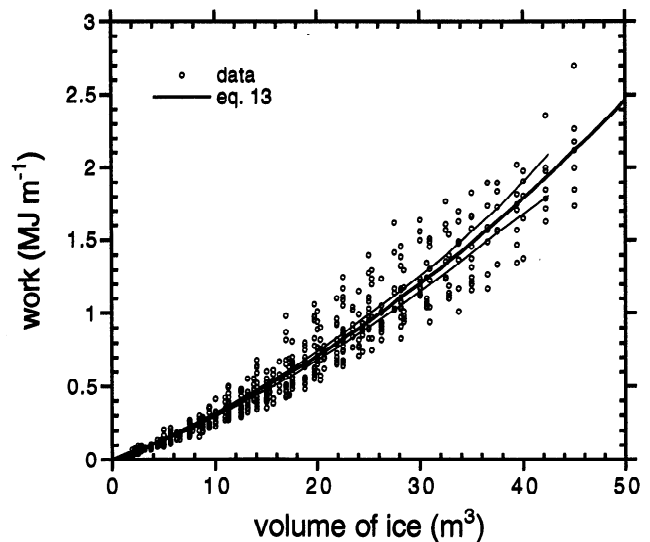


Figure 12. Total energy consumption (megajoules per meter) versus volume of ridged ice. The data points are from sets of seven experiments with ice of six thicknesses calculated at regular intervals during each experiment. Equation (13) is plotted within a 95% confidence interval.

**Table 4.** Comparison of Block Length-to-Thickness Ratios, Average Sail Heights, and Sail and Keel Slopes Between Numerical Ridge Experiments and Field Data

<i>h</i> , m	<i>L/h</i>	<i>L/h*</i>	<i>H</i> , m	<i>H*</i> , m	$\theta_1$ , deg	$\theta_2$ , deg	$\phi_1$ , deg	$\phi_2$ , deg
0.20	5.05	5.65	1.10	1.66	21	16	39	41
0.25	4.57	4.92	1.35	1.86	12	15	43	57
0.30	3.90	4.33	1.67	2.03	20	18	37	48
0.35	3.40	4.09	1.72	2.19	12	24	32	59
0.40	3.30	3.85	2.00	2.35	10	31	42	58
0.45	3.07	3.64	2.12	2.49	19	15	40	60

Abbreviations are *h*, block thickness; *L/h*, length-to-thickness ratio; *H*, average sail heights;  $\theta_1$ , leaidside sail slopes;  $\theta_2$ , floeside sail slope;  $\phi_1$ , leaidside keel slope; and  $\phi_2$ , floeside keel slope.

\*These values are computed from field data of *Tucker et al.* [1984]. All other values are from numerical ridge experiments.

$$d\text{Work}/dPE = (927.80V + 26126)/(61.76V + 2107.26). \tag{16}$$

The ratio given by (16) increases with volume from an initial value of 12.4 to 13.96 at a volume of 50 m<sup>3</sup> (per meter).

The ratio of work to the increase in potential energy is used in finite difference models of the Arctic Basin [*Hibler*, 1980; *Flato*, 1991] to determine the bulk strength of the ice pack *p\**. *Hibler* [1980] and *Flato* [1991] determine *p\** from an equation,

$$p^* \text{ div } \mathbf{v} = c \int h^2 \psi(h) dh, \tag{17}$$

developed by *Thorndike et al.* [1975] and *Rothrock* [1975], wherein the rate of work by compressive deformation is equated to the rate of increase of potential energy due to ridging. In the equation, *div v* is the divergence, *c* is a constant that depends on the density of ice and seawater, and  $\psi(h)$  is the ice thickness redistribution function. However, this equation neglects the energy dissipated during ridge creation. *Hibler* [1980] and *Flato* [1991] account for dissipation by multiplying the right side of (17) by an assumed ratio of the rate of work to the rate of increase of potential energy. Since the estimation of energy dissipation applies to a large area of the ice pack, the ratio used should be an average value over many ridges in various stages of creation. It is worth noting that *Flato* obtained the best match between recorded buoy tracks and simulations using a value of 15.

**Block Lengths and Ridge Slopes**

Field measurements of first-year ridge sails have been made by *Tucker et al.* [1984] and *Kovacs* [1972], among

**Table 5.** Effects of Ice Friction on Block Length-to-Thickness Ratios, Average Sail Heights, and Sail and Keel Slopes

$\mu$	$\mu_w$	<i>L/h</i>	<i>H</i>	$\theta_1$	$\theta_2$	$\phi_1$	$\phi_2$
1.0	0.6	3.90	1.67	20	16	38	41
0.8	0.6	3.67	1.76	17	22	34	46
0.6	0.6	3.89	1.94	14	19	38	58
0.4	0.6	4.28	1.77	16	26	31	38
1.0	0.3	3.96	1.94	20	38	35	35
0.8	0.3	4.06	2.00	21	28	29	50
0.6	0.3	4.44	2.30	18	26	29	36
0.4	0.3	4.66	2.20	27	15	22	17

Definitions and values are same as those in Tables 2 and 4.

others. The measurements have included sail heights and slopes and block length-to-thickness ratios. A comparison between field data of *Tucker et al.* [1984] and the simulated ridges is given in Table 4. The length-to-thickness ratios *L/h* are averages obtained from the final configurations of seven experiments with ice of each given thickness. The sail heights *H* (meters) and slopes (degrees) were measured from the average profiles shown in Figure 10. The angles  $\theta_1$  and  $\theta_2$  pertain to the leaidside and floeside sail slopes, respectively. The angles  $\phi_1$  and  $\phi_2$  pertain to the leaidside and floeside keel slopes. The slope angle measurements were made from lines drawn by eye through the major portion of each slope. The length-to-thickness ratio *L/h\** is from the equation  $L = 2.04h + 0.72$ , and the sail height *H\** is from the equation  $H = 3.71h^{0.5}$  of *Tucker et al.*, based on field measurements. *Tucker et al.* measured an average sail slope of 25.1°. *Kovacs* [1972] reported an average sail slope of 24° and an average keel slope of 38°.

In Table 5 the effects of friction on the ridge measurements is shown. Again, the length-to-thickness ratios are averages obtained from the final configurations of seven experiments, with each set of friction coefficients using lead ice with a thickness of 30 cm. The heights and slopes were measured from the average profiles shown in Figure 8. The smaller, underwater friction coefficient is associated with longer blocks, larger sails, and steeper sail slopes.

**Conclusions**

The intent of this work is to dynamically model pressure ridge formation in situations where relatively thin, first-year ice is driven against a thick floe. The main assumption in this study is that the ice sheet breaks in flexure (including buckling). Therefore the conclusions should not be applied to ice thicknesses where the dominant failure mechanism is crushing.

The simulations of ridge growth begin with a sheet of intact lead ice pushed at constant speed against a floe. The ice sheet breaks repeatedly in flexure, piling against, under, and on top of the floe, to create the ridge structure. This study has shown that a particularly important feature of the structure is the accumulation of floating rubble in front of the floe. This part of the keel acts as a platform to support the downward component of the sail-building force. The simulations show that the ridging process is an alternation between sail building and keel building. In general, sail building continues until the sheet buckles or the platform collapses under the increasing sail-building force. Rubble is added to the keel at the surface, and it grows like a pile of granular material, albeit, inverted.

The results demonstrate that the above-water friction coefficient determines the relative volumes of the sail and keel. This happens because the magnitude of the sail-building force, which depends on both the friction coefficient and the sail volume, is limited by buckling. Therefore since the available force is limited, increasing the friction coefficient will cause a reduction in the sail volume. Furthermore, for a given volume of ridged ice a reduction in sail volume will be accompanied by an equal increase in keel volume. An increase in the above-water friction coefficient had the paradoxical effect of reducing the total energy consumption. However, the variation in energy consumption over a wide range of above-water friction coefficients for a given underwater coefficient was approximately 15%. The underwater coefficient affected the slope of the keel and had a small effect on energy consumption.

The energetics of pressure ridging depend strongly on the thickness of the lead ice sheet. The results of experiments with ice of various thicknesses, in which the friction coefficients are fixed, can be reduced to a single plot of energy consumed versus the volume of ridged ice. This is because the average profiles are similar with respect to volume. This conclusion applies to a state, termed primary ridge growth, in which the maximum sail height has not yet been reached. Quadratic curves were found by regression that closely fit the data for total energy consumed and potential energy of the ridge structure as functions of ridged ice volume. The average ridge-building force as a function of ice volume was obtained from the derivative of the total energy equation.

In large-scale sea ice modeling [Hibler, 1980; Flato, 1991], using a variable thickness approach, it is convenient to parametrize the total rate of energy consumption in ridging in terms of the rate of increase of potential energy. The results of this study yield ratios of energy consumption to potential energy between 9.6 and 16.8, depending on friction and ice thickness. The results also indicate that for a given ice thickness and set of friction coefficients the ratio remains nearly constant over the period of primary ridge growth.

**Acknowledgments.** I would like to thank the Office of Naval Research for the opportunity to do this work, and I would like to thank Jackie Richter-Menge, Steve Ackley, George Ashton, and the

anonymous reviewers for their help in preparing this manuscript for publication.

## References

- Flato, G. M., Numerical investigation of the dynamics of a variable thickness Arctic ice cover, Ph.D. thesis, Thayer School of Engineering, Dartmouth College, Hanover, N. H., 1991.
- Hibler, W. D., III, Modeling a variable thickness sea ice cover, *Mon. Weather Rev.*, *108*, 1943–1973, 1980.
- Hopkins, M. A., Numerical simulation of systems of multitudinous polygonal blocks, *Rep. 92-22*, Cold Reg. Res. and Eng. Lab., Hanover, N. H., 1992.
- Hopkins, M. A., and W. D. Hibler III, On the ridging of a thin sheet of lead ice, *Ann. Glaciol.*, *15*, 81–86, 1991.
- Hopkins, M. A., W. D. Hibler III, and G. M. Flato, On the numerical simulation of the sea ice ridging process, *J. Geophys. Res.*, *96*, 4809–4820, 1991.
- Kovacs, A., On pressured sea ice, paper presented at International Conference on Sea Ice, Icelandic Natl. Res. Council, Reykjavik, 1972.
- Mellor, M., Mechanical behavior of sea ice, in *The Geophysics of Sea Ice*, edited by N. Untersteiner, pp. 165–281, Plenum, New York, 1986.
- Parmeter, R. R., and M. D. Coon, Model of pressure ridge formation in sea ice, *J. Geophys. Res.*, *77*, 6565–6575, 1972.
- Perloff, W. H., and W. Baron, *Soil Mechanics Principles and Applications*, Ronald, New York, 1976.
- Rothrock, D. A., The energetics of the plastic deformation of pack ice by ridging, *J. Geophys. Res.*, *80*, 4514–4519, 1975.
- Sayed, M., and R. M. W. Frederking, Stresses in first-year pressure ridges, paper presented at International Offshore Mechanics and Arctic Engineering Symposium, Am. Soc. of Mech. Eng., Tokyo, 1984.
- Thorndike, A. S., D. A. Rothrock, G. A. Maykut, and R. Colony, The thickness distribution of sea ice, *J. Geophys. Res.*, *80*, 6565–6575, 1975.
- Tucker, W. B., III, D. S. Sodhi, and J. W. Govoni, Structure of first-year pressure ridge sails in the Prudhoe Bay region, in *The Alaskan Beaufort Sea: Ecosystems and Environment*, edited by P. W. Barnes, D. M. Shell, and E. Reimnitz, pp. 115–135, Academic, San Diego, Calif., 1984.
- Walton, O. R., Particle-dynamics modeling of geological materials, *Rep. UCRL-52915*, Lawrence Livermore Lab., Univ. of Calif., Livermore, 1980.

M. A. Hopkins, Ice Engineering Research Branch, Cold Regions Research and Engineering Laboratory, 72 Lyme Road, Hanover, NH 03755. (e-mail:hopkins@hanover-crrl.army.mil)

(Received March 14, 1994; accepted April 12, 1994.)